High color-rendering flat lamps using quantum-dot color conversion films

Jiun-Yi Lien,[†,¶] Chih-Jung Chen,[‡,¶] Ray-Kuang Chiang,[∗,‡] and Sue-Lein Wang[∗,†]

Department of Chemistry, National Tsing Hua University, Hsinchu 30013, Taiwan, Republic of China, and Nanomaterials Laboratory, Far East University, Hsing-Shih, Tainan 74448, Taiwan, Republic of China

E-mail: rkc.chem@msa.hinet.net; slwang@mx.nthu.edu.tw

Abstract

Colloidal quantum dots are promising next-generation phosphors to enhance the color rendition of light-emitting devices (LEDs) while minimizing the brightness drop. In order to exploit the beneficial tunability of quantum dots for highly efficient devices, optimization and determination of the performance limit are of crucial importance. In this work, a facile preparation process of red-emission quantum dot films and simulation algorithm for fitting this film with two commercial LED flat lamps to the optimized performance are developed. Based on the algorithm, one lamp improves from cold-white light (8669 K) with poor color rendition ($R_a = 72$) and luminous efficacy (85 lm/W) to warm-white light (2867 K) with $R_a = 90.8$ and $R_9 = 74.9$, and the other reaches $R_a = 93 \sim 95$. Impressively, the brightness drop is only about $15 \sim 20\%$. Furthermore, our device shows reliability over 1000 hours with only PET (polyethylene-terephthalate) films as the barrier, indicating that this auxiliary red-emission film can be easily applied to improve the color rendition of most commercial LED flat lamps.

[∗]To whom correspondence should be addressed
[†]Department of Chemistry, National Tsing Hua University, Hsinchu 30013, Taiwan, Republic of China
[‡]Nanomaterials Laboratory, Far East University, Hsing-Shih, Tainan 74448, Taiwan, Republic of China
[¶]Contributed equally to this work

Introduction

Semiconducting nanocrystals, also called quantum dots (QDs), have attracted great attention due to promising applications such as light-emitting diodes (LEDs), solar cells, and biosensors.[1–4] For applications of lighting and displays, QDs can be utilized to enhance the color rendition of white-LED lamps[5,6] and the color gamut of liquid-crystal displays.[7–9] Compared with traditional phosphors, the QDs are with advantages of high efficiency, tunable emission wavelength, narrow bandwidth, and low-cost solution-synthesis. However, with wide absorption spectra and nano-scale sizes, reabsorption and Förster resonance energy transfer (FRET) could induce the problems of color shift and efficiency drop, depending on the device structure.[10–12] Other issues like photo-oxidization[13,14] and thermal quench[15,16] also limit QD applications. Many strategies have been adapted to avoid these issues, e.g., the remote-phosphor designs.[17]

In the field of solid-state lighting, it is crucial for indoor illumination to generate warm-white light with correlated color temperature (CCT) lower than 4000 K while maintaining high color rendition and high luminous efficacy (LE). Theoretically, it can be generated by four-color LEDs to reach the color-rendering index (CRI) with $R_a = 90$ and the highest luminous efficacy of radiation (LER) being 408 lm/W$_{opt}$, provided that the intensity ratios and wavelengths of the four colors are given correctly.[18] Due to the green gap of LED technology, high cost of additional control circuits, and different lifetimes of individual chips, the devices using multiple chips are inferior to the ones using a blue-emitting chip together with multiple phosphors.[19] It was predicted that, by employing QD phosphors, a LED has the potential to achieve LER larger than 380 lm/W$_{opt}$ and LE being 256 lm/W with perfect light recycle and extraction efficiency.[20–22]

Although the electrical-to-optical power conversion efficiency of commercial blue-emitting chips is improved every year, the LE of current lighting devices (using traditional phosphors, QDs, or both) is still far from the theoretical limit to date.[17,23,24] Besides the imperfect down-conversion and light-extraction efficiencies of phosphors and QDs, multiple-color mixing also causes the problems of reabsorption and FRET.[11,25–27] In order to simultaneously meet the demands of CCT, CRI, and LE, optimization of the wavelength, bandwidth, and quantity of QDs has to be reached for var-

ious optical structures and phosphor compositions with limited efficiencies. However, to our best knowledge, there is still no such an optimization method available in the literature.

In this work, we develop an algorithm for optimization by determining the optical path of QD absorption and the external quantum efficiency (EQE) of QD emission. We also produce the desired quantum-dot color-conversion films (QDCCFs) and apply them to two commercial flat lamps of cold-white light (CCT = 8669 K, labeled as lamp-1) and day-white light (CCT = 5792 K, labeled as lamp-2). By employing a simple film-type structure, we achieve warm-white light (CCT = 2867 K) with $R_a > 90$, $R_9 > 70$ for the strong red color, and *wall-plug* LE = 68 lm/W, better than most reported phosphor-based technologies.[3] More importantly, the drop of brightness due to lowering the CCT is limited to only 15 ∼ 20% without modification of the basic structure of the lamps. Our device also shows excellent stability and can be directly applied to most of commercial LED flat lamps.

Results and discussion

Well-dispersed QD-polymer film

The commercial flat lamps used in our experiment consist of a traditional edge-light structure with a diffuser film to enhance the uniformity of light, as shown in Fig. 1(a). For the warm-white light application, the QDCCFs are simply inserted between the light-guide plate and diffuser film. The QDCCFs were fabricated by creating a homogeneously dispersed QD-polymer composite [Fig. 1(b)], where the functionalized co-polymer containing a small amount of methacrylic acid (1%) was designed to increase the affinity to QD surfaces[28] and QDs are tightly held on the polymer chains for dispersion.[26] The QD-polymer composite is sealed by two polyethylene-terephthalate (PET) films to reduce photo-oxidation, and the flexibility of QDCCFs is improved by adding 24 wt% Lauryl methacrylate (LMA) in the co-polymer, as shown in Fig. 1(c). In addition, the zinc-oxide (ZnO) scattering particles are dispersed inside the QD-polymer layer in order to enhance the light-extraction efficiency from the guiding modes.[29–32]

3

(a) diffuser

QDCCF

cold-white light

light-guide plate

(b) QD/toluene QD/polymer/toluene
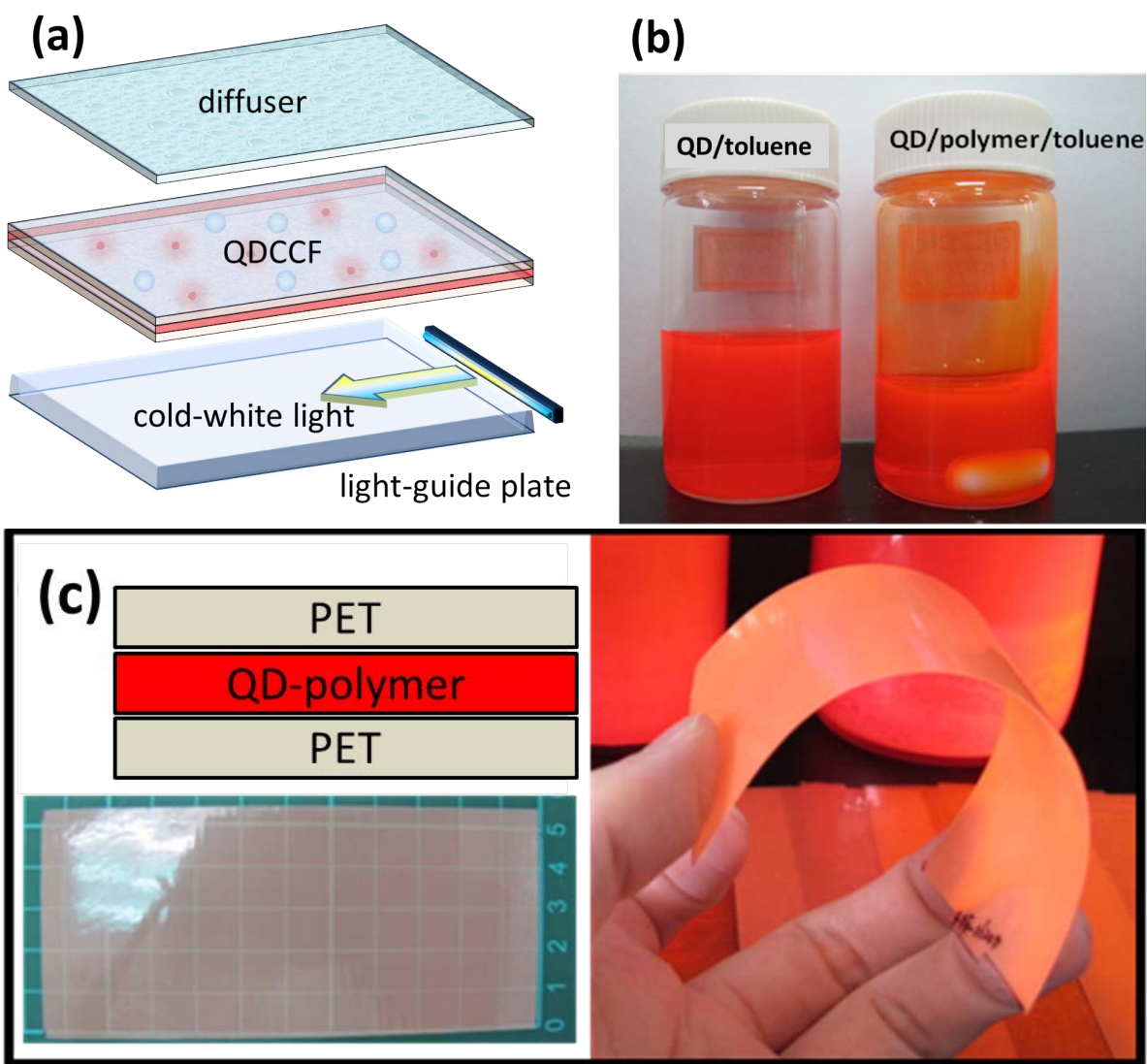
(c) PET

QD-polymer

PET

Figure 1: (a) Device structure of the warm-white flat lamps employing the QDCCFs. (b) Photographs of well dispersed QDs in toluene and toluene-polymer solutions. (c) Demonstration of the structure and flexibility of the QDCCFs.
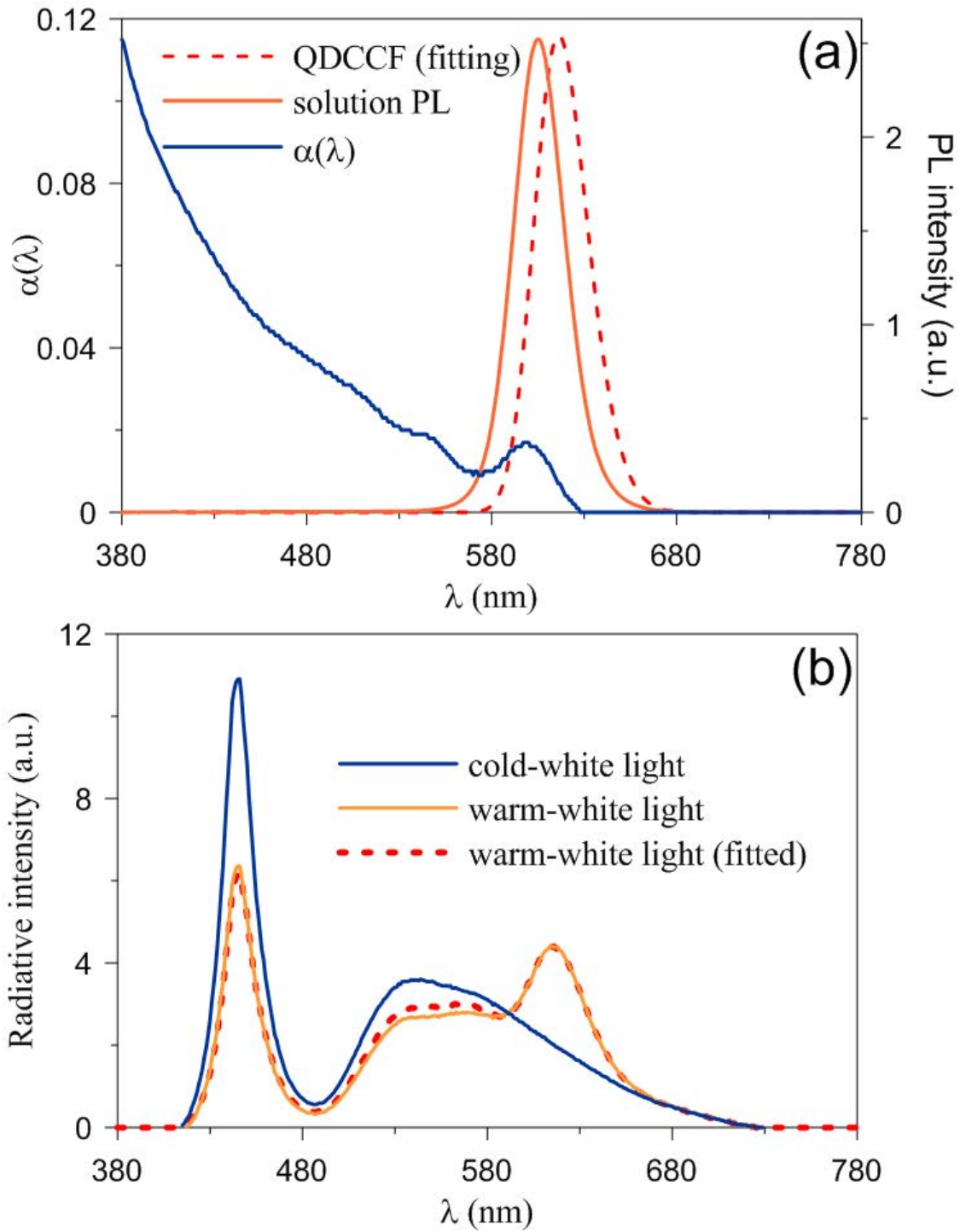
Figure 2: (a) The measured attenuation coefficient $\alpha(\lambda)$ and photoluminescent intensity of a dilute QD solution for the test sample (blue and orange solid curves), as well as the fitted red emission of the test QDCCF (dashed curve) with red shift about 6 nm. (b) The energy spectra of the input cold-white light (blue solid curve), the measured warm-white light of the test sample (orange solid curve), and the fitted warm-white light derived from our simulation algorithm (dashed red curve).

Optimization algorithm

For demonstration of our optimization scheme, the QDCCFs are applied to lamp-1 of cold-white light (CCT $= 8669$ K) with poor colorimetric ($R_a = 72$) and photometric (LE $= 85$ lm/W) performance. The scheme is based on the color-conversion process of QDCCFs, where partial cold-white light is absorbed by QDs and down-converted into red emission. According to the Beer-Lambert law, the transmission spectrum $T_{cw}(\lambda)$ of the cold-white light with wavelength λ satisfies

$$T_{cw}(\lambda) = 10^{-A(\lambda)} = 10^{-\alpha(\lambda)\rho l(\lambda)}, \tag{1}$$

where the absorbance $A(\lambda)$ is proportional to the attenuation coefficient $\alpha(\lambda)$ and the concentration ρ of the QDs, as well as the optical path $l(\lambda)$ inside the device. The absorbed photon number N_{abs} is determined by

$$N_{abs} = \int [1 - T_{cw}(\lambda)] n_{cw}(\lambda) d\lambda, \tag{2}$$

where $n_{cw}(\lambda)$ is the photon-density spectrum of the cold-white light. Therefore, the down-converted photon number N_{emit} is given by

$$N_{emit} = \eta_{EQE} \times N_{abs} = \eta_{QY} \times \eta_{ext} \times N_{abs}$$
$$= \int n_r(\lambda) d\lambda, \tag{3}$$

where $n_r(\lambda)$ is the photon-density spectrum of the red emission, η_{EQE} is the external quantum efficiency of QDCCFs, η_{QY} is the photoluminescent quantum yield of QDs, and η_{ext} is the *effective* light-extraction efficiency of the films. The energy spectrum of the warm-white light $E_{ww}(\lambda)$ is therefore determined by both the spectra of transmitted cold-white light $[1 - T_{cw}(\lambda)]E_{cw}(\lambda)$ and

red emission $E_r(\lambda)$, i.e.,

$$E_{ww}(\lambda) = [1 - T_{cw}(\lambda)] E_{cw}(\lambda) + E_r(\lambda)$$
$$\equiv \{[1 - T_{cw}(\lambda)] n_{cw}(\lambda) + n_r(\lambda)\} \left(\frac{hc}{\lambda}\right), \tag{4}$$

where h is the Plank constant and c is the speed of light.

In order to achieve maximum colorimetric or photometric performance with a given CCT range, we have to determine the appropriate absorbance $A(\lambda)$ and red emission $n_r(\lambda)$ of the QD-CCFs. For $A(\lambda)$, the attenuation coefficient $\alpha(\lambda)$ can be determined by the absorbance of a dilute solution of the QDs, and the concentration ρ is predetermined before fabricating the QDCCFs. The optical path length $l(\lambda)$ depends on the film thickness, the density of scattering particles, the recycle mechanism of the device, etc. Ignoring the small dispersion of the refractive indices of the device inside the optical regime, l is approximately independent of the wavelength of the cold-white light and to be determined.

The red-emission spectrum $n_r(\lambda)$ of the warm-white device cannot be determined by the photoluminescence spectra of either the QDCCFs or solutions due to a strong red shift.[26] This red shift results from FRET and guiding-induced reabsorption inside a film, and it is further enhanced by the recycle mechanism of the light-guide plate. However, we can simulate $n_r(\lambda)$ by a skew-normal distribution $f_{sn}(\lambda)$, i.e.,

$$n_r(\lambda) = \eta_{EQE} \times N_{abs} \times f_{sn}(\lambda) \tag{5}$$
$$f_{sn}(\lambda) = \frac{2}{\Delta_r} \phi\left(\frac{\lambda - \lambda_r}{\Delta_r}\right) \Phi\left(\gamma\left(\frac{\lambda - \lambda_r}{\Delta_r}\right)\right),$$

where $\phi(x)$ is the standard normal probability density function and $\Phi(x)$ is the corresponding cumulative distribution function. Here γ is a parameter controlling the skewness of the distribution. The parameters λ_r and Δ_r are related (not identical, due to the skewness) to the peak wavelength (λ_R) and the full width at half maximum (FWHM, Δ_R) of the red emission. The approximation of

skew-normal distribution describes the band tail of a solid-state phosphor, and it can be generally applied to monodispersed QDs and many phosphors with a single emission level.

The unknown parameters l, γ, λ_r, Δ_r, and η_{EQE} can be determined by fitting the energy spectrum $E_{ww}(\lambda)$ of a test QDCCF, as shown in Fig. 2. The thickness of the test QDCCF (QD-polymer layer) is about 45 μm, and the emission wavelength/FWHM (λ_R/Δ_R) given by γ, λ_r, and Δ_r is 616/34 nm, which is red-shifted about 6 nm from that of the same QDs inside a dilute solution [see Fig. 2 (a)]. The external quantum efficiency η_{EQE} of the test sample is about 69%. For the QDs of the test sample, the quantum yield (η_{QY}) is about 90%, and the effective light-extraction efficiency η_{ext} can be estimated as 77%. The optical path length l is proportional to the film thickness with fixed QD density and device structure, and thus we can find an optimized thickness by tuning l. Another way to control the absorbance $A(\lambda)$ is to tune the QD density ρ. However, increasing ρ leads to a further red shift and the reduction of η_{EQE} due to reabsorption and FRET. Thus we optimize the QDCCF with a fixed ρ of 1 wt% for simplicity.

From Fig. 2 (b), the only deviation of the measured spectrum is the slightly reduced yellow emission from LED phosphors, compared with the calculated spectrum. This is because of that a small part of the blue light recycled by the light-guide plate and diffuser film to excite the yellow emission is absorbed by the QDCCF. Although this effect leads to an overestimation of LE, we will see later that all the trends of photometric and colorimetric performance can be well predicted and used to optimize the QDCCF.

Optimized warm-white-light devices

The simulated properties with various film thickness and emission wavelength λ_R of the QDCCFs are shown in Fig. 3, based on the parameters derived from the test sample of warm-white light and the input cold-white light. In general, both LE and CCT decrease with increasing film thickness [Fig. 3 (a)-(d)]. The CRIs increase with film thickness to their maximum values, and then drop slowly due to deviation from the reference black-body radiation. Compared with the experiments, all colorimetric properties are well predicted by our simulation. The overestimation of LEs
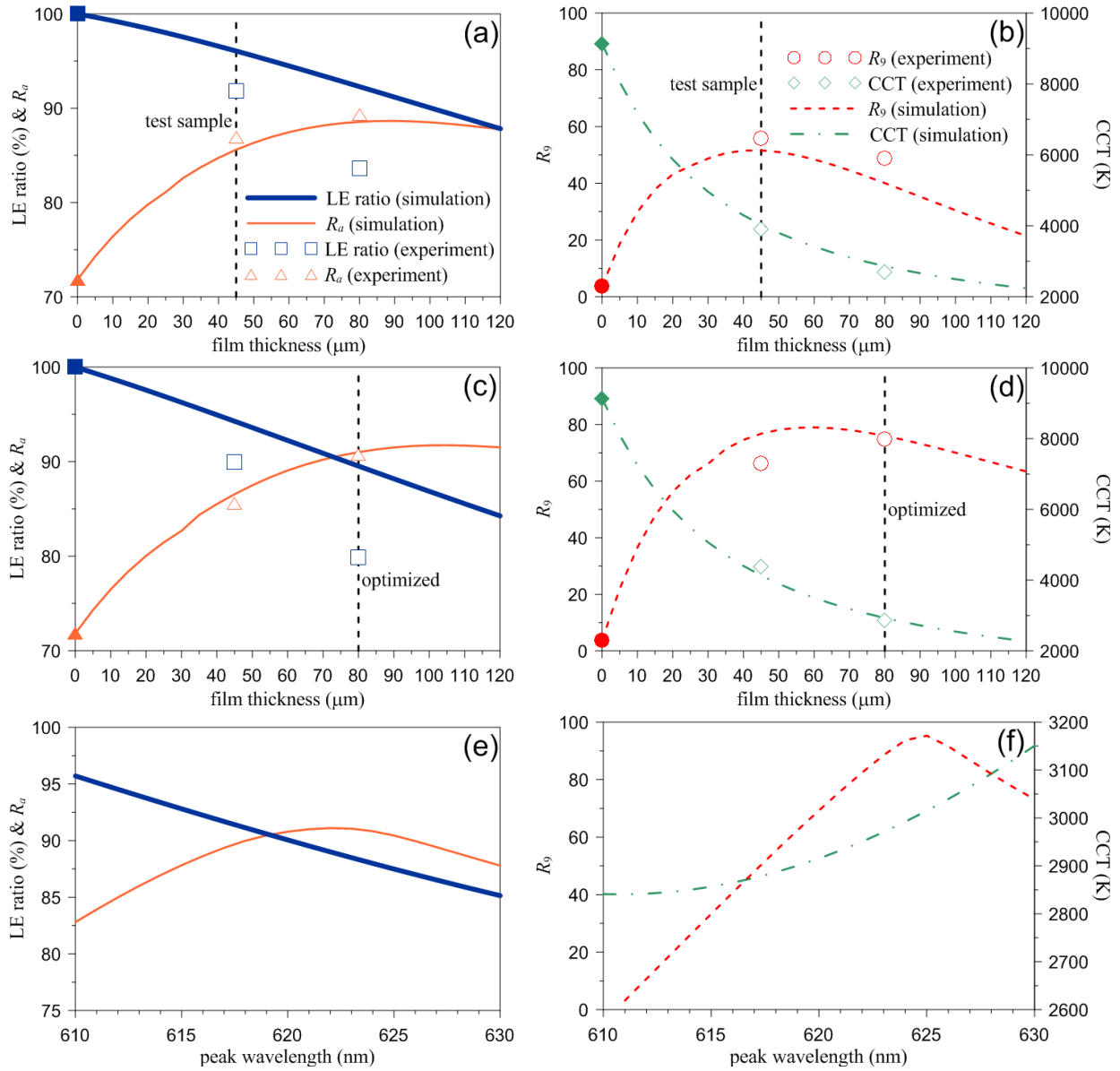
Figure 3: (a)-(d) Simulation of photometric (LE ratio with respect to the input cold-white light) and colorimetric performance as functions of the film thickness of the QDCCFs, where the wavelength (λ_R) of red emission is 616 nm for (a)-(b) and 621 nm for (c)-(d), respectively. (e)-(f) The same simulation as functions of λ_R, with the film thickness being fixed at 80 μm. For comparison, the experimental data are also shown by discrete symbols. The data of input cold-white light are represented as filled symbols, while those of the test sample and other samples for verification are represented as empty symbols.

increases with film thickness due to that more recycled blue light is shared with the QDCCF. However, the resulting dropping trends of LE simulation are consistent with the experimental ones, and is sufficient to determine the optimal thickness.

Our goal is to achieve $R_a \geq 90$ and $R_9 \geq 70$ with the largest LE. Using the same QDs of 616 nm emission as the test sample, the maximum R_a is about 88.7 with thickness 90 μm, and thus the emission wavelength of the QDCCF must be further tuned. From the simulation of wavelength effects in Fig. 3 (e)-(f), the LE decreases with increasing λ_R because of the contribution of luminosity function of human visual perception. The CCT slightly increases with λ_R and can be controlled around 3000 K with film thickness $70 \sim 80$ μm. The general color rendering index R_a reaches 90 only for λ_R in the range of $619 \sim 625$ nm. Moreover, the red-color rendering index R_9 can be significantly enhanced to above 70 for $\lambda_R = 621 \sim 630$ nm, and it even reaches 95 for $\lambda_R = 625$ nm. Therefore, we prepared a QDCCF with the desired wavelength about 621 nm with film thickness 80 μm, which is already shown in Fig. 3 (c)-(d). This optimized sample exhibits $R_a = 90.8$, $R_9 = 74.9$, CCT = 2867 K, and LE = 68 lm/W (80% brightness compared with the cold-white light of lamp-1).

Figure 4 (a) compares the measured and simulated spectra of the optimized warm-white light of lamp-1. Besides the deviation of the yellow-phosphor emission in these spectra, the red emission in the measured spectrum is also weaker than that in the simulated one. This is due to the lower quantum yield ($\eta_{QY} \approx 80\%$) of the QDs used for the QDCCF with $\lambda_R = 621$ nm, leading to that η_{EQE} decreases to a value of 60%. If $\eta_{QY} > 90\%$, the resulting LE can be larger than 70 lm/W. Nevertheless, this simple device has shown better performance and efficiency than that of most other warm-white light technologies and even most QD-LEDs,[3] without modifying the chip efficiency, the phosphor composition, and the light-guide structure of the commercial lamp. This indicates the importance of this optimization procedure in conjunction with the feasible tunability of QDs.

We also applied the QDCCFs to lamp-2 of day-white light (5792 K) with better colorimetric performance ($R_a = 83.7$ and $R_9 = 14.8$). Following the same optimization procedure, we have

achieved warm-white light (3549 K) with $R_a = 93.2$ and $R_9 = 55.3$, as shown in Fig. 4(b). With $\lambda_R = 617$ nm, the brightness drop reduces to 15% due to less CCT difference between the day-white and warm-white light. Furthermore, the colorimetric performance can be improved to $R_a = 95.1$ and $R_9 = 78.6$ with $\lambda_R = 622$ nm and CCT= 3305 K. Although the brightness drop of the sample of $R_a = 95.1$ is 27%, the reason is not only the larger emission wavelength, but also the lower η_{QY} of the corresponding QDs. Our simulation shows that lamp-2 has the potential to achieve $R_a = 96$ and $R_9 = 96$ with limited brightness drop about $20 \sim 25\%$ as λ_R is shifted to 630 nm.

By exploiting the flat-lamp structure, our optimized devices also show excellent reliability, as shown in Fig. 4(b). The PET-protected QDCCF was assembled into the flat-lamp module and tested with 4 W electrical power under ambient conditions over 1000 hours, where the photoluminescent (PL) intensity, CCT, and CRIs remain unchanged from the initial performance. From a previous report, [17] without the PET protection, the emission of QDs quenches after 300 hours even for a remote-phosphor structure. The operating temperature of QDCCF is about 45 °C, slightly higher than the room temperature (30 °C) due to down-conversion-induced heat. The successful fabrication of reliable high-CRI flat lamps with the robust QDCCFs is quite encouraging with regard to the development of next-generation lighting sources.

Performance limits of QDCCFs

Table 1: Optimization for given η_{EQE}.

η_{EQE} (%)	λ_R (nm)	Δ_R ($\geq$ 20 nm)	film thickness (μm)	LE ratio (%)	CCT	R_a	R_9
50	619	20	81	85.8	3139	90	72
60	618	20	70	90.6	3197	90	68
70	617	20	63	94.1	3157	90	65
80	617	22	59	96.6	3141	90	67
90	617	29	57	98.8	3089	90	63
100	618	34	56	100.8	3030	90	60

We also estimated the limit of the device performance based on lamp-1, which could be further improved by tuning the FWHM (Δ_R) and external quantum efficiency (η_{EQE}) of the QDCCFs.
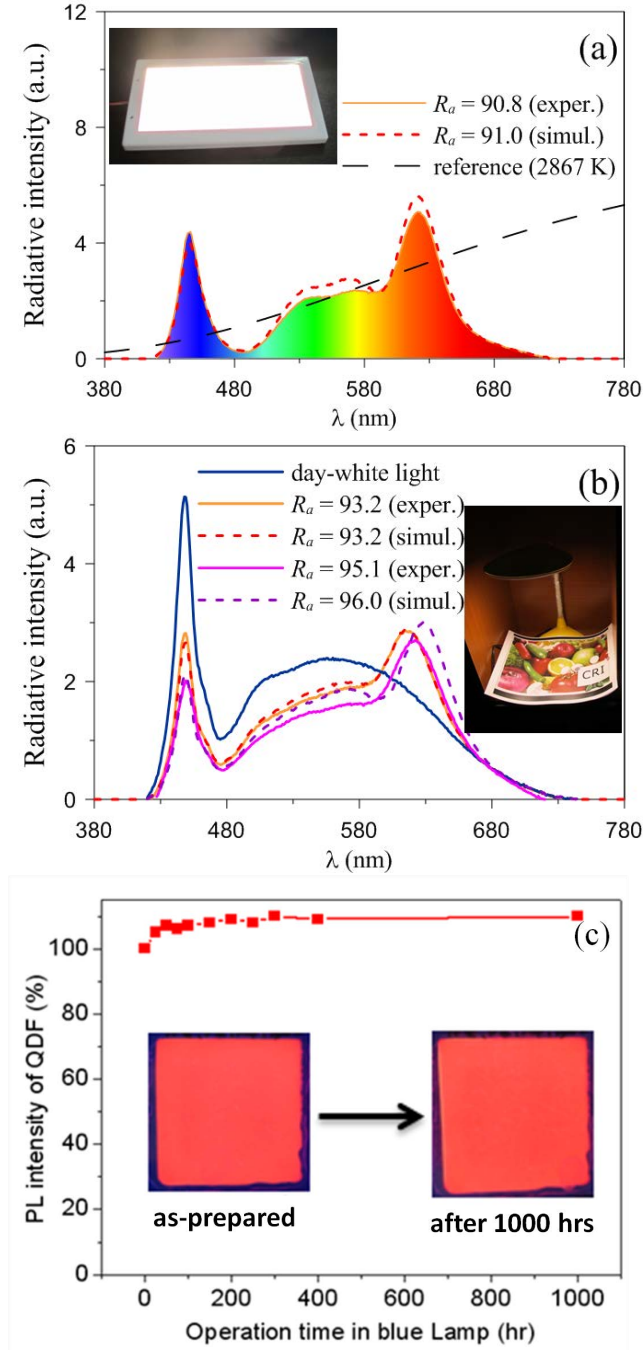
Figure 4: (a) Measured energy spectrum (orange solid curve) of the optimized warm-white light of lamp-1 with $R_a = 90.8$, $R_9 = 74.9$, CCT = 2867 K, and 20% brightness drop compared with the input cold-white light, which is based on our simulation (red dashed curve). The black long-dashed curve represents the reference light with CCT = 2867 K. The QDCCF is prepared with emission wavelength/FWHM (λ_R/Δ_R) 621/34 nm and film thickness 80 μm. (b) Spectra of the input day-white light (blue solid curve) and the measured (solid curves) as well as the simulated (dashed curved) warm-white light of lamp-2. (c) Time-dependent PL intensity of the QDCCF, where the red emission keeps initial intensity for over 1000 hours. The insets in (a) and (b) demonstrate the respective optimized devices.

For a critical situation, the minimum Δ_R of contemporary QDs is about 20 nm.[33] The advantage of small Δ_R of QDs compared with that of traditional phosphors is to avoid energy waste in the deep-red region. Meanwhile, the whole spectrum needs to be as continuous as possible to keep high color rendition. Our algorithm provides a way to study this trade-off and suggests an optimal value of Δ_R. The external quantum efficiency of a QDCCF is dominated by η_{QY} of the QDs and the design of film structure. Its improvement reduces the cost of QDs and matrix materials, and enhances the LE of the warm-white light devices. Besides improving η_{QY}, the light-extraction efficiency from guiding modes can be enhanced by modifying the surface structure such as diffuser attachment, microlens (or prism) structures, distributed Bragg reflectors, and photonic crystals.[34] However, these factors strongly depend on the synthesis process of QDs and manufacturability of QDCCFs.

Table 1 shows the optimal λ_R, Δ_R (with minimum value of 20 nm), and film thickness for given η_{EQE}, where R_a is required to be 90 with largest LE ratio with respect to the input cold-white light. If Δ_R is smaller than that of our samples, the peak wavelength can be shorter than 621 nm, with thinner film thickness and larger LE. For lower η_{EQE}, the bandwidth is required to be as narrow as possible to achieve the specification with the largest LE. If η_{EQE} is higher than 80%, the optimal Δ_R becomes larger than 20 nm, and the LE could be almost the same as the input cold-white light.

Summary

In summary, we developed a simulation algorithm for optimizing QD-based light-emitting devices. We also practically fabricated quantum-dot color conversion films applied to two commercial white-light lamps for validation of the simulation. Under this simple flat-lamp structure, our devices show excellent reliability over 1000 hours and are expected to extend to various commercial products. The first optimized device achieves warm-white light with $R_a = 90.8$, $R_9 = 74.9$, and only 20% brightness drop (68 lm/W) due to lowering the color temperature. The second device can be designed either for excellent color rendition with $R_a = 95.1$ and $R_9 = 78.6$ or for lower

brightness drop about 15% with $R_a = 93.2$ and $R_9 = 55.3$. The algorithm can be easily applied to other devices such as LEDs with remote phosphors or with on-chip phosphor package for desired CCT or individual CRIs (R_i, $i = 1 \sim 15$). It is also useful for QD backlight units of liquid-crystal displays with given spectra of color filters, target white point, and color gamut. Optimization essentially plays a significant role of QD-based technologies, which can highlight the feasible tunability of QDs for higher photometric and colorimetric performance. Thus our work paves the way for high-quality QD-based lighting and display devices.

Experimental

Chemicals

CdZnSeS/ZnS core/shell quantum dots (Taiwan Nanocrystals Inc.), sub-micrometer ZnO powder (99%, Showa), methyl methacrylate (MMA, 99%, Aldrich), LMA (96%, Aldrich), acrylic acid (MA, 99%, Aldrich), azobisisobutyronitrile (AIBN, 99%, Aldrich) were used in an as-received condition without further purification.

The CdZnSeS/ZnS core/shell QDs were chosen with emission wavelength $605 \sim 615$ nm, FWHM 33 nm, and PL quantum yield about $80 \sim 90\%$. Figure 5(a) shows the transmission-electron-microscopy (TEM) image of QDs with emission wavelength 609 nm and average size 6.5 ± 0.3 nm. The selected area electron diffraction (SAED) patterns [inserted in Fig. 5(a)] and high-resolution TEM [HRTEM, Fig. 5(b)] image reveal a high-quality zinc-blende (ZB) structure of the QDs. The atomic composition of the QDs is identified as 23.6% Cd, 12.3% Se, 27.9% Zn, and 36.2% S, from the energy-dispersive spectroscopy (EDS) shown in Fig. 5(c).

Fabrication of QDCCF

In the fabrication of QDCCFs, QDs (0.02 g), ZnO powder (0.02 g), $PMMA_{0.75}$-$LMA_{0.24}$-co-$MA_{0.01}$ (1.98 g), and toluene (7 mL) were mixed in a 20 mL flask by a magnetic stirrer for 1

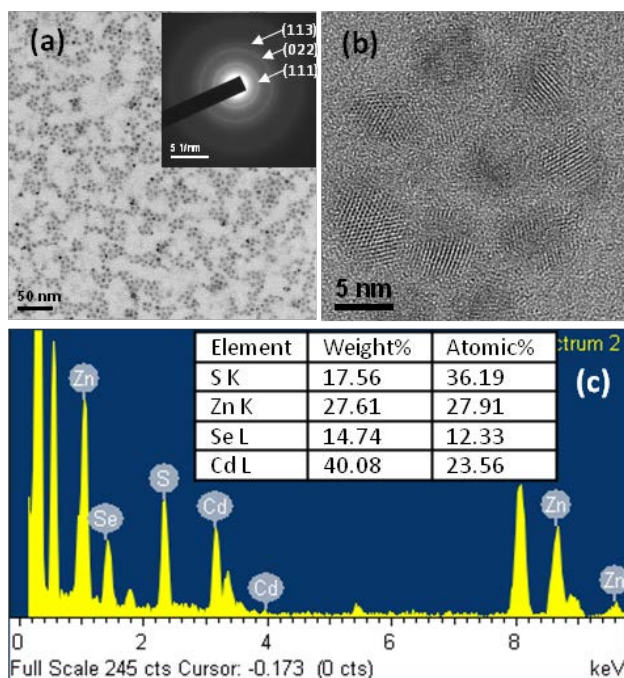| Element	Weight%	Atomic%
S K	17.56	36.19
Zn K	27.61	27.91
Se L	14.74	12.33
Cd L	40.08	23.56

Figure 5: (a) TEM and (b) HRTEM micrographs of the CdZnSeS/ZnS QDs with emission wavelength of 609 nm. The SAED pattern inserted in (a) shows a zinc-blende structure of the QDs. (c) EDS patterns of the CdZnSeS/ZnS QDs.

day at room temperature. The QD-polymer-toluene solution (8 mL) was poured onto a PET-based release film. The QD films were formed by a blade coating machine and dried at room temperature for 1 hour and then at 60 °C for 4 hours for removal of free toluene solvent. The thickness of the film can be controlled between 40 to 100 μm. Finally, the dry film was encapsulated in the middle of two PET (20 μm) films by a laminating machine to avoid the contact with water and oxygen.

Acknowledgement

References

(1) Wood, V.; Bulović, V. Colloidal quantum dot light-emitting devices. *Nano Rev.* **2010**, *1*, 5202.

(2) Kim, J. Y.; Voznyy, O.; Zhitomirsky, D.; Sargent, E. H. 25th anniversary article: colloidal

quantum dot materials and devices: a quarter-century of advances. *Adv. Mater.* **2013**, *25*, 4986–5010.

(3) Shirasaki, Y.; Supran, G. J.; Bawendi, M. G.; Bulović, V. Emergence of colloidal quantum-dot light-emitting technologies. *Nat. Photon.* **2013**, *7*, 13–23.

(4) Bera, D.; Qian, L.; Tseng, T.-K.; Holloway, P. H. Quantum dots and their multimodal applications: a review. *Materials* **2010**, *3*, 2260–2345.

(5) Nizamoglu, S.; Zengin, G.; Demir, H. V. Color-converting combinations of nanocrystal emitters for warm-white light generation with high color rendering index. *Appl. Phys. Lett.* **2008**, *92*, 031102.

(6) Nizamoglu, S.; Erdem, T.; Sun, X. W.; Demir, H. V. Warm-white light-emitting diodes integrated with colloidal quantum dots for high luminous efficacy and color rendering. *Opt. Lett.* **2010**, *35*, 3372–3374.

(7) Jang, E.; Jun, S.; Jang, H.; Lim, J.; Kim, B.; Kim, Y. White-light-emitting diodes with quantum dot color converters for display backlights. *Adv. Mater.* **2010**, *22*, 3076–3080.

(8) Luo, Z.; Xu, D.; Wu, S.-T. Emerging quantum-dots-enhanced LCDs. *J. Disp. Technol.* **2014**, *10*, 526–539.

(9) Zhu, R.; Luo, Z.; Chen, H.; Dong, Y.; Wu, S.-T. Realizing Rec. 2020 color gamut with quantum dot displays. *Opt. Express* **2015**, *23*, 23680–23693.

(10) Kagan, C. R.; Murray, C. B.; Nirmal, M.; Bawendi, M. G. Electronic energy transfer in CdSe quantum dot solids. *Phys. Rev. Lett.* **1996**, *76*, 1517–1520.

(11) Jang, H. S.; Yang, H.; Kim, S. W.; Han, J. Y.; Lee, S.-G.; Jeon, D. Y. White light-emitting diodes with excellent color rendering based on organically capped CdSe quantum dots and Sr_3SiO_5:Ce^{3+},Li^+ phosphors. *Adv. Mater.* **2008**, *20*, 2696–2702.

(12) Akselrod, G. M.; Prins, F.; Poulikakos, L. V.; Lee, E. M. Y.; Weidman, M. C.; Mork, A. J.; Willard, A. P.; Bulović, V.; Tisdale, W. A. Subdiffusive exciton transport in quantum dot solids. *Nano Lett.* **2014**, *14*, 3556–3562.

(13) Hines, D. A.; Becker, M. A.; Kamat, P. V. Photoinduced surface oxidation and its effect on the exciton dynamics of CdSe quantum dots. *J. Phys. Chem. C* **2012**, *116*, 13452–13457.

(14) Hines, D. A.; Kamat, P. V. Recent advances in quantum dot surface chemistry. *ACS Appl. Mater. Interfaces* **2014**, *6*, 3041–3057.

(15) Zhao, Y.; Riemersma, C.; Pietra, F.; Koole, R.; de Mello Donegá, C.; Meijerink, A. High-temperature luminescence quenching of colloidal quantum dots. *ACS Nano* **2012**, *6*, 9058–9067.

(16) Cai, X.; Martin, J. E.; Shea-Rohwer, L. E.; Gong, K.; Kelley, D. F. Thermal quenching mechanisms in II-VI semiconductor nanocrystals. *J. Phys. Chem. C* **2013**, *117*, 7902–7913.

(17) Moon, J. W.; Kim, J. S.; Min, B. G.; Kim, H. M.; Yoo, J. S. Optical characteristics and longevity of quantum dot-coated white LED. *Opt. Mater. Express* **2014**, *4*, 2174–2181.

(18) Phillips, J. M.; Coltrin, M. E.; Crawford, M. H.; Fischer, A. J.; Krames, M. R.; Mueller-Mach, R.; Mueller, G. O.; Ohno, Y.; Rohwer, L. E. S.; Simmons, J. A.; Tsao, J. Y. Research challenges to ultra-efficient inorganic solid-state lighting. *Laser Photon. Rev.* **2007**, *1*, 307–333.

(19) Krames, M. R.; Shchekin, O. B.; Mueller-Mach, R.; Mueller, G. O.; Ling, Z.; Harbers, G.; Craford, M. G. Status and future of high-power light-emitting diodes for solid-state lighting. *J. Disp. Technol.* **2007**, *3*, 160–175.

(20) Erdem, T.; Nizamoglu, S.; Sun, X. W.; Demir, H. V. A photometric investigation of ultra-efficient LEDs with high color rendering index and high luminous efficacy employing nanocrystal quantum dot luminophores. *Opt. Express* **2010**, *18*, 340–347.

(21) Zhong, P.; He, G.; Zhang, M. Optimal spectra of white light-emitting diodes using quantum dot nanophosphors. *Opt. Express* **2012**, *20*, 9122–9134.

(22) Erdem, T.; Nizamoglu, S.; Demir, H. V. Computational study of power conversion and luminous efficiency performance for semiconductor quantum dot nanophosphors on light-emitting diodes. *Opt. Express* **2012**, *20*, 3275–3295.

(23) Song, W.-S.; Lee, S.-H.; Yang, H. Fabrication of warm, high CRI white LED using non-cadmium quantum dots. *Opt. Mater. Express* **2013**, *3*, 1468–1473.

(24) Kim, J.-H.; Song, W.-S.; Yang, H. Color-converting bilayered composite plate of quantum-dot-polymer for high-color rendering white light-emitting diode. *Optics Letters* **2013**, *38*, 2885–2888.

(25) Demir, H. V.; Nizamoglu, S.; Erdem, T.; Mutlugun, E.; Gaponik, N.; Eychmüller, A. Quantum dot integrated LEDs using photonic and excitonic color conversion. *Nano Today* **2011**, *6*, 632–647.

(26) Chen, C.-J.; Lin, C.-C.; Lien, J.-Y.; Wang, S.-L.; Chiang, R.-K. Preparation of quantum dot/polymer light conversion films with alleviated Förster resonance energy transfer redshift. *J. Mater. Chem. C* **2015**, *3*, 196–203.

(27) Lee, K.-H.; Han, C.-Y.; Kang, H.-D.; Ko, H.; Lee, C.; Lee, J.; Myoung, N.; Yim, S.-Y.; Yang, H. Highly efficient, color-reproducible full-color electroluminescent devices based on red/green/blue quantum dot-mixed multilayer. *ACS Nano* **2015**,

(28) Tamborra, M.; Striccoli, M.; Curri, M. L.; Alducin, J. A.; Mecerreyes, D.; Pomposo, J. A.; Kehagias, N.; Reboud, V.; Sotomayor Torres, C. M.; Agostiano, A. Nanocrystal-based luminescent composites for nanoimprinting lithography. *Small* **2007**, *3*, 822–828.

(29) Ryu, B. D.; Uthirakumar, P.; Kang, J. H.; Kwon, B. J.; Chandramohan, S.; Kim, H. K.; Kim, H. Y.; Ryu, J. H.; Kim, H. G.; Hong, C.-H. Enhanced light output power of GaN-based

light-emitting diodes by nano-rough indium tin oxide film using ZnO nanoparticles. *J. Appl. Phys.* **2011**, *109*, 093116.

(30) Yang, X.; Dev, K.; Wang, J.; Mutlugun, E.; Dang, C.; Zhao, Y.; Liu, S.; Tang, Y.; Tan, S. T.; Sun, X. W.; Demir, H. V. Light extraction efficiency enhancement of colloidal quantum dot light-emitting diodes using large-scale nanopillar arrays. *Adv. Funct. Mater.* **2014**, *24*, 5977–5984.

(31) Mao, P.; krishna Mahapatra, A.; Chen, J.; Chen, M.; Wang, G.; Han, M. Fabrication of polystyrene/ZnO micronano hierarchical structure applied for light extraction of light-emitting devices. *ACS Appl. Mater. Interfaces* **2015**, *7*, 19179–19188.

(32) Shin, C.-H.; Shin, E. Y.; Kim, M.-H.; Lee, J.-H.; Choi, Y. Nanoparticle scattering layer for improving light extraction efficiency of organic light emitting diodes. *Opt. Express* **2015**, *23*, A133–A139.

(33) Wang, A.; Shen, H.; Zang, S.; Lin, Q.; Wang, H.; Qian, L.; Niu, J.; Song Li, L. Bright, efficient, and color-stable violet ZnSe-based quantum dot light-emitting diodes. *Nanoscale* **2015**, *7*, 2951–2959.

(34) Zhmakin, A. Enhancement of light extraction from light emitting diodes. *Phys. Rep.* **2011**, *498*, 189 – 241.

Graphical TOC Entry